electronic reprint

Acta Crystallographica Section A
Foundations of Crystallography
ISSN 0108-7673

Accurate triplet phase determination in non-perfect crystals – a general phasing procedure

Sérgio L. Morelhão

Acta Crystallographica Section A
Foundations of Crystallography
ISSN 0108-7673

Received 2 May 2003
Accepted 27 June 2003

Accurate triplet phase determination in non-perfect crystals – a general phasing procedure

Sérgio L. Morelhão

Instituto de Física, USP, CP 66318, 05315-970 São Paulo, SP, Brazil. Correspondence e-mail: morelhao@if.usp.br

A completely different approach to the problem of physically measuring the invariant triplet phases by three-beam X-ray diffraction is proposed. Instead of simulating the three-beam diffraction process to reproduce the experimental intensity profiles, the proposed approach makes use of a general parametric equation for fitting the profiles and extracting the triplet phase values. The inherent flexibility of the parametric equation allows its applicability to be extended to non-perfect crystals. Exploitation of the natural linear polarization of synchrotron radiation is essential for eliminating systematic errors and to provide accurate triplet phase values. Phasing procedures are suggested and demonstrative examples from simulated data are given.

1. Introduction

Invariant triplet phases contain important pieces of information about crystalline structures. It is well known that the *n*-beam diffraction (*n*-BD) of X-rays in crystals can lead to physical measurements of reflection phases, more precisely to the invariant triplet phases. Experimental procedures and diffraction theories have been developed and improved for decades in order to achieve a better understanding of the *n*-BD phenomenon (Hart & Lang, 1961; Colella, 1974; Post, 1977; Chang, 1982; Høier & Marthinsen, 1983; Juretschke, 1986; Tischler & Batterman, 1986; Shen, 1986; Shen & Colella, 1987; Weckert & Hümmer, 1997; Stetsko *et al.*, 2001; Thorkildsen *et al.*, 2001; and many others). Nevertheless, there are still several difficulties in this research field that require further attention. One major difficulty occurs because the principle of the *n*-BD phase sensitivity relies on the interference of multiple diffracted waves inside the crystal. Since the diffracted waves have to preserve structural phase information, the diffraction theories capable of reproducing the *n*-BD interference of the waves describe the diffraction process in perfect crystals. When a phase value is extracted by fitting the characteristic interference profiles of the *n*-BD with such theories, it is implicitly assumed that the crystal is perfect or, in other words, that all counted/recorded photons have interacted with the perfect periodic lattice. What are the errors due to such an assumption? How does the interference profile change if some photons are scattered around crystalline defects by slightly displaced atoms? What level of crystalline perfection is required for phasing? To answer these questions, it is necessary to describe the defect structures of the crystals or to include arbitrary lattice displacements in the available theories, as, for example, considered by Larsen & Thorkildsen (1998) or as recently suggested by Okitsu (2003). However, independently of the theoretical approach used to describe the *n*-beam diffraction, and even restricted to three-beam diffraction in perfect crystals, the equations and their solutions are very complex.

Since the description of the *n*-BD process in real samples is so troublesome, would it be possible to obtain the triplet phase without having to describe the diffraction process precisely? For the sake of comparison, let us discuss the strategy to obtain accurate diffraction peak positions. When the required information is the peak position (two-beam cases or powder diffraction), what is the usual procedure? If the peak profile is a Gaussian, a Lorentzian or any other function, one fits the experimental data with the appropriate function and extracts the position with good accuracy, adjusting the height and width of the peak. It is not always necessary to make use of precise diffraction theories that produce the observed peak profile to measure its position. Why was not a similar strategy attempted to obtain the triplet phases? The answer is because a general parametric function capable of fitting the three-beam diffraction profiles was not yet established. Actually, such a parametric function is available but its potential has not been clearly emphasized. The contribution of this paper relies on the possibility of determining the triplet phases by just analyzing the interference profiles.

Recently, during an investigation of the interference profiles of three-beam diffraction (3-BD) cases as a function of the relative intensity of the diffracted beams (Morelhão & Kycia, 2002), some disagreement between experimental and theoretical profiles were observed. The set of profiles of the same 3-BD case obtained at different intensity ratios, *i.e.* different states of linear polarization (Morelhão & Avanci, 2001), requires a diffraction theory that allows all experimental profiles to be reproduced with a common triplet phase value. The attempt to simulate the set of profiles with the standard

well known second-order Born approximation, or just second-order approximation, of the 3-BD (Shen, 1986; Shen & Colella, 1988; Chang & Tang, 1988), the simplest available approach, has failed. However, the behavior of the experimental profiles, as a function of polarization, indicates that they could be reproduced by including two new parameters in the equation derived from the second-order approximation. These two empirical parameters were physically justified, without a detailed discussion of their theoretical basis, as evidence of crystalline defects in the diffracting volume of the sample and as higher-order corrections. Under a critical review, the incompleteness of the used approach compromises a conclusion on the presence or not of crystalline defects, and on the systematic errors that they generated. The aim of this paper is to provide some theoretical basis to the inclusion of these two parameters and to propose a general parametric equation to reproduce the 3-BD profiles. Evidence is given that this equation allows, to some extent, a quantitative description of crystalline defects into the 3-BD profiles and an accurate triplet phase determination in perfect as well as non-perfect crystals. Suggestions of general phasing procedures, for which algorithms can be developed, are also given.

2. Three-beam X-ray diffraction

In the framework of the second-order approximation, when a 3-BD is excited by the incident X-rays, each diffracted beam is a sum of two wavefields, $\mathbf{E}_P$ and $\mathbf{E}_D$. The primary wave $\mathbf{E}_P$ is produced by a single reflection (reflection A) while the other wave, $\mathbf{E}_D$, also called the detoured wave, comes from a double-bounce reflection formed by reflection B plus the coupling reflection C, whose indices are given by A–B. By keeping one wave excited and changing the angular condition of the other, the characteristic interference profiles are obtained. The most common is the interference profile obtained by an azimuthal scan (φ scan) of the sample, where the intensity $I(\varphi) \propto |\mathbf{E}_P + \mathbf{E}_D(\varphi)|^2$ is a function of the crystal rotation around the diffraction vector of the reflection A. Since the primary wave is kept excited during the φ rotation, its intensity is taken as constant in this approach. $I(\varphi)$ can also be written as

$$I(\varphi) \propto |\mathbf{E}_P|^2 + |\mathbf{E}_D(\varphi)|^2 + 2|\mathbf{E}_P||\mathbf{E}_D(\varphi)| \cos\gamma \cos(\Delta\Psi), \quad (1)$$

where γ is the angle between the oscillation directions of the $\mathbf{E}_P$ and $\mathbf{E}_D$ wavefields. The total phase difference, $\Delta\Psi$, between these two waves is the sum of two phase angles: the invariant phase triplet $\delta_T = \delta_B + \delta_C - \delta_A$, where δ_G is the phase of the structure factor of reflection G (= A, B or C), and the dynamical phase shift $\Omega(\varphi)$ of the resonant term, the term that describes the excitation of the secondary wave due to the crystal rotation (Weckert & Hümmer, 1997; Shen *et al.*, 2000). In other words, $\Delta\Psi = \Omega(\varphi) + \delta_T$, where $\Omega(\varphi)$ is known from the X-ray diffraction theory and δ_T is the desired triplet phase value to be determined from experiments.

Equation (1) provides an easy-to-understand description of the 3-BD phenomenon, but it is incomplete. Only two possible paths, or channels (Shen, 1986), have been considered for the incident photons inside the crystal: a photon is scattered either by reflection A or by the detour reflection $B + C$. In fact, there is a dynamical balance of energy among the diffracted beams as they travel through the crystal, which is precisely described by the n-beam dynamical theory of X-ray diffraction. In conventional two-beam diffraction, the dynamical balance occurs between diffracted–reflected and diffracted–transmitted beams. For instance, if only reflection A (indices hkl) is excited, the photons can be scattered by reflection A and then by reflection $\bar{A}$ (indices $\bar{h}\bar{k}\bar{l}$) and then by reflection A again, and so on. The different number of bounces suffered by each photon before emerging from the crystal defines the different possible channels for the photons. Under 3-BD, the situation is identical but the channels are not limited to those between the diffracted–reflected (A or B) and diffracted–transmitted beams. The energy balance also occurs between the A and B diffracted–reflected beams; and the coupling reflection C is responsible for such balance. For example, the photons in the diffracted beam A could have been scattered by any of the following '*Umweg*' channels: A (reflection A), $B + C$, $A + \bar{A} + A$, $B + \bar{B} + A$, $A + \bar{C} + C$, $A + \bar{A} + B + C$, $B + \bar{B} + B + C$, $B + C + \bar{C} + C$, ...; *i.e.* channels where the resultant diffraction vector is the same as reflection A. When the anomalous dispersion of all atoms in the crystal is negligible, *i.e.* when Friedel's law applies, the phases of the photons scattered by these channels are δ_A or $\delta_B + \delta_C$. Otherwise, small deviations in the phase values may occur to each channel. Channels like B, $A + \bar{C}$, $A + \bar{A}$, $B + C + \bar{C}$, ..., those where the resultant diffraction vector is null or is the same as reflection B, are responsible for the intensities of the other diffracted beams (secondary and diffracted–transmitted beams) and, consequently, for some reduction in the intensity of beam A. This is also known as the *Aufhellung* effect (Wagner, 1923). Hereafter, the diffraction channels are classified within two categories: *Umweg* and *Aufhellung* channels, the former being those responsible for the structural phase information in the 3-BD profiles. [The *Umweg* terminology, also used by other authors, has been borrowed from the word *Umweganregung*, first employed to name the enhancement of a diffracted beam due to simultaneous diffraction inside a single crystal (Renninger, 1937).]

3. Traditional concept of crystalline imperfection in diffraction theories

In X-ray crystallography, the reduction of power owing to rescattering of diffracted beams inside a perfect periodic lattice has been called primary extinction. The rescattering is the occurrence of any diffraction channel with more than one bounce. A traditional concept, derived from intensity measurements in two-beam diffraction experiments, is that primary extinction depends on the size of the diffracting lattice. The smaller the lattice is, the smaller is the probability for the photons to be scattered by channels with higher numbers of bounces. If the crystal is so small that only single-bounce channels have non-negligible probabilities, n-BD does not occur and the kinematical theory of X-ray diffraction is applied. On the other hand, for large crystals where the probabilities of all channels cannot be neglected, the dy-

namical theory of X-ray diffraction is required for describing the diffraction process.

Real crystals are in general made of several perfectly diffracting regions, usually called mosaic blocks. Structural phase determination by 3-BD in such crystals is possible, in principle, if primary extinction occurs inside some of the blocks. Otherwise, the energy transfer among the diffracted beams takes place by secondary extinction owing to channels where the bounces occur in difference blocks. In these cases, the structural phase information is lost because of the unpredictable positioning of the blocks.

4. Theoretical consideration for feasible phasing of non-perfect crystals

Theoretical descriptions of diffraction processes in generalized defective crystals are complicated, and might be useless for practical phasing applications. However, restricted to single crystals with low levels of point and line defects, it can be quite simple. To clearly introduce this simple description, an imaginary experiment is presented below. It allows an analogy to the modification that will be implemented in the second-order approximation, equation (1), for fitting any interference profile from a perfect crystal to a non-perfect crystal.

In this imaginary experiment, consider two monochromatic X-ray beams, with a phase difference of $\Delta\zeta$, propagating along the same direction, and that both beams can be turned on or off independently. P_1 and P_2 are the detector readings (power of the beams) measured for each beam when the other is off. S_1 and S_2 are the respective areas of the beams at the detector eye, then the intensities of the beams are $I_1 = P_1/S_1$ and $I_2 = P_2/S_2$. The electric fields of these beams are parallel to each other and their moduli proportional to $(I_1)^{1/2}$ and $(I_2)^{1/2}$. If we assume that the beams have a partial overlap given by S_{12}, the superposition area of the beams ($S_{12} = S_1 \cap S_2$), what is the detector reading P when both beams are turned on?

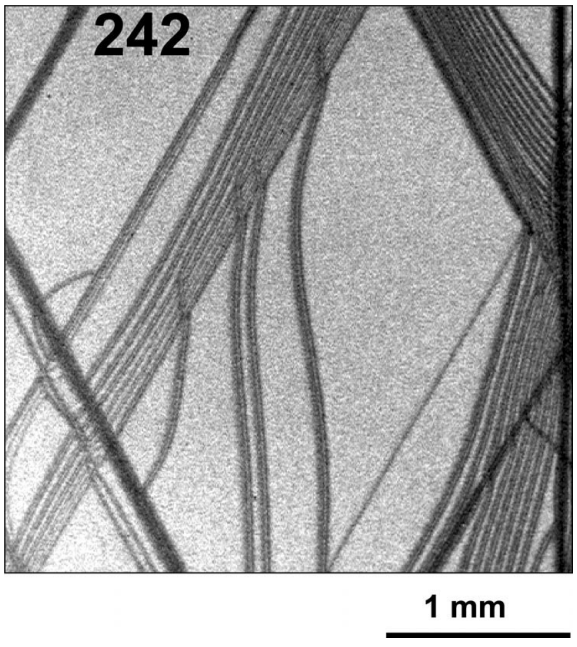

Figure 1
Synchrotron white-beam X-ray topography from a slab of silicon (111) crystal revealing dislocations on the slip system of {111} planes. After Morelhão *et al.* (2000).

There are two distinct contributions to P: one from the parts of the beams that do not overlap, $(S_1 - S_{12})I_1$ and $(S_2 - S_{12})I_2$, and another from the part that interferes, $S_{12}[I_1 + I_2 + 2(I_1)^{1/2}(I_2)^{1/2}\cos\Delta\zeta]$. In terms of the detector readings of each beam, $P_1 = I_1S_1$ and $P_2 = I_2S_2$, the resultant reading is

$$P = P_1 + P_2 + 2[(S_{12}/S_1)(S_{12}/S_2)]^{1/2}(P_1)^{1/2}(P_2)^{1/2}\cos\Delta\zeta. \quad (2)$$

It allows us to conclude that the correct value of the resultant reading is obtained when *the interference term is multiplied by the square root of the interfering fractions of the beams, i.e. the fractions of the beams that are capable of interfering.*

Relevant questions for structural phasing by the 3-BD phenomenon are related to physical reasons that reduce the capability of interference between two parallel and overlapping ($S_1 = S_2 = S_{12}$) X-ray diffracted beams. One physical reason for such a reduction is easily understood by analyzing an X-ray topography image, such as the one shown in Fig. 1. The total integrated intensity, P, of this image has contributions from white areas as well as from dark lines observed all across the image. If these contributions are counted separately as $P_{\rm dark}$ and $P_{\rm white}$, $P = P_{\rm dark} + P_{\rm white}$ where $P_{\rm dark} = \alpha P$, $P_{\rm white} = (1 - \alpha)P$ and α gives the weight of each type of contribution. White areas have a lower intensity owing to primary extinction since they correspond to diffraction in a perfect periodic lattice, *i.e.* dynamical diffraction. The scattered photons from these white areas do preserve structural phase information. The dark lines are produced by displaced atoms owing to the strain field around the core of the dislocations. Since each atom is displaced from its periodic position in the lattice by slightly different amounts over the range of the strain field that goes over several wavelengths, there is no structural phase information from the strong kinematical contributions of the dark lines. When X-ray detectors are used instead of imaging techniques, the detector reading is equivalent to the integrated intensity over the area of the diffracted beam. But, unfortunately, detectors do not discriminate white and dark contributions. Then, to avoid an equivocal assumption, it is better to suppose that only a fraction of the detector reading – usually called beam intensity – is capable of interfering with another diffracted beam.

When two parallel beams are excited in the same volume of the crystal, exactly as assumed by the second-order approximation, the interference term of these beams is multiplied by $[(1 - \alpha_P)(1 - \alpha_D)]^{1/2}$, which is the square root of the interfering fractions of the primary (A) and detoured ($B + C$) beam intensities. Since in most cases no theoretical calculation or experimental measurement can account for the exact values of α_P and α_D, the best option is to replace the square root by a

single unknown parameter, labeled ξ. Then, (1) can be rewritten in a more appropriate form as

$$P(\varphi) = P_P + P_D(\varphi) + 2\xi[P_D(\varphi)]^{1/2}(P_P)^{1/2}\cos\gamma\cos(\Delta\Psi), \quad (3)$$

where P_P and $P_D(\varphi)$ are the detector readings for the primary and detoured beams, respectively. ξ is in the range from 0 to 1, *i.e.* $0 \le \xi \le 1$. For reasons that are given below, it is convenient to split equation (3) into two components, $P(\varphi) = P_\sim(\varphi) + P_\wedge(\varphi)$, where

$$P_\sim(\varphi) = P_P + \xi^2 P_D(\varphi) + 2\xi[P_D(\varphi)]^{1/2}(P_P)^{1/2}\cos\gamma\cos(\Delta\Psi) \quad (4a)$$

and

$$P_\wedge(\varphi) = (1-\xi^2)P_D(\varphi). \quad (4b)$$

The $P_\sim(\varphi)$ component preserves the expected asymmetry of the interference profile for a given phase triplet. As ξ is reduced from unity, this asymmetric undistorted phase-sensitive component decreases while the symmetrical component, $P_\wedge(\varphi)$, increases. In this decomposition, it has been assumed that any asymmetry of the profile is due to interference effects between the diffracted beams, and that $P_D(\varphi)$ is a symmetrical function [see equation (8)].

The modified second-order approximation, summarized by (3), has the flexibility to take into account, to some extent, the presence of crystalline defects in the diffracting volume of a crystal. This is possible by means of the parameter ξ, which reflects the fact that some of the diffracted photons have random phases due to their interaction with the defective lattice; the average effect of such photons is just to increase the counting rates of the diffracted beams. In terms of phase determination, this parameter generates systematic errors due to symmetrical distortion of the interference profiles, quantified by $P_\wedge(\varphi)$. Certainly, the parameter ξ preserves its physical meaning in 3-BD cases where the scattering of the A and $B + C$ channels are very dominant over the scattering of the other channels, however, they do not represent the majority of the cases. Even if equation (3) is applicable to all *Umweg* cases, it represents a restricted set of cases that could be analyzed by this equation.

5. General equation for fitting three-beam diffraction profiles of linearly polarized X-rays

To extend the applicability of equation (3) to cases where the effects of the *Aufhellung* channels are significant, an extra symmetric negative component can be added to $P_\wedge(\varphi)$, as experimentally demonstrated by Morelhão & Kycia (2002). And, for fitting purposes, equation (3) can be converted into the following parametric form

$$P(\varphi) = v_P^2[1 - b|f(\varphi)|^2] + R^2|f(\varphi)|^2 v_D^2 + 2\xi R|f(\varphi)|v_P v_D\cos\gamma\cos(\Omega + \delta_T), \quad (5)$$

which can also be split into asymmetric and symmetric components as

$$P_\sim(\varphi) = v_P^2 + \xi^2 R^2|f(\varphi)|^2 v_D^2 + 2\xi R|f(\varphi)|v_P v_D\cos\gamma\cos(\Omega + \delta_T) \quad (6a)$$

and

$$P_\wedge(\varphi) = [(1-\xi^2)R^2 v_D^2 - b v_P^2]|f(\varphi)|^2. \quad (6b)$$

The polarization coefficients, v_P and v_D, depend on the direction of the diffracted beams, $\mathbf{k}_{A,B}$ (Fig. 3), as well as on the polarization direction, $\hat{e}$, of the incident beam, $\mathbf{k}_0$. They are calculated by

$$\mathbf{v}_P = -\hat{k}_A \times (\hat{k}_A \times \hat{e})$$

and

$$\mathbf{v}_D = \hat{k}_A \times \{\hat{k}_A \times [\hat{k}_B \times (\hat{k}_B \times \hat{e})]\}, \quad (7)$$

then, $v_P^2 = \mathbf{v}_P \cdot \mathbf{v}_P$, $v_D^2 = \mathbf{v}_D \cdot \mathbf{v}_D$ and $v_P v_D \cos\gamma = \mathbf{v}_P \cdot \mathbf{v}_D$ ($v_{P,D} = |\mathbf{v}_{P,D}|$). The minus sign in $\mathbf{v}_P$ was missing in previous papers (Morelhão & Kycia, 2002; Morelhão, 2003). R^2 is the maximum ratio between the primary and detoured intensities without polarization coefficients; if $P_P = X v_P^2$ is the measured intensity of the primary beam for a given state of linear polarization, the maximum intensity of the detoured beam will be $P_D(\varphi_0) = X R^2 v_D^2$ since $|f(\varphi_0)|^2 = 1$. In the normalized equations above, (5) or (6), $X = 1$.

$$f(\varphi) = \{\pm w/[2(\varphi - \varphi_0) \mp iw]\} = |f(\varphi)|\exp[i\Omega(\varphi)] \quad (8)$$

is the line profile function used to describe the excitation of the detour reflection, *i.e.* of the *Umweg* channels, with the φ rotation. This function has been chosen because it meets two major requirements: (i) a symmetric Lorentzian-like profile of $P_D(\varphi)$, experimentally observed when the primary reflection is very weak or forbidden, therefore, $|f(\varphi)|^2$ is a Lorentzian function centered at φ_0 and with a FWHM equal to w; and (ii) $\Omega(\varphi)$ is 0 [$f(\varphi) = |f(\varphi)|$] or 180° [$f(\varphi) = -|f(\varphi)|$] when the reciprocal-lattice point of reflection B is inside or outside the Ewald sphere. The + and − signs in the numerator (− and + in the denominator) stand for the 'out → in' and 'in → out' cases, respectively. Across the surface of the Ewald sphere, $\Omega(\varphi)$ behaves almost like the hyperbolic tangent function proposed by Shen *et al.* (2000). It is also a practical approximation of the true phase function, as seen in dynamical diffraction theory (Authier, 1986). Comparisons between these phase shift functions and their effects on some interference profiles are shown in Fig. 2. Small discrepancies are seen, even though $f(\varphi)$ as proposed in equation (8) is chosen because it saves computer time. It is a very simple function and provides at the same time the profile $|f(\varphi)|$ and the phase shift $\Omega(\varphi)$. There is no need to program one function to reproduce the profile and another function to account for the phase shift. As will be pointed out later, computer time is an important issue to determine δ_T by fitting procedures.

The b parameter in (5) and (6*b*) stands for the *Aufhellung* effect. It has a positive or zero value ($b \ge 0$) and it produces a symmetric negative distortion in the interference profile that is proportional to the intensity of the primary beam, *i.e.* b is the fraction of *Aufhellung* with respect to the intensity of beam A. Here, *Aufhellung* has been assumed to have the same profile, $|f(\varphi)|^2$, of the detour reflection. There is no straightforward demonstration of this assumption, but it is a reasonable

approximation because the angular condition for *Aufhellung* is the same as the detour reflection or, in other words, *Umweg* and *Aufhellung* channels are excited simultaneously.

The validity of (5) to describe the underlying physics of any 3-BD process is questionable since no assumption on diffraction geometry, absorption and crystal shape are involved. However, despite all the physical arguments used to obtain its final form, (5) can be seen as a general parametric equation for fitting 3-BD profiles, where correction due to physical effects such as primary extinction (dynamical diffraction that already includes *Aufhellung* channels) and imperfections are compensated by adjusting the R, ξ and b parameters, as well as the intrinsic width w. As far as the asymmetries in the interference profiles are ruled by diffracted photons from *Umweg* channels, *i.e.* by $\cos(\Omega + \delta_T)$, the profiles can be reproduced by (5). There is one obvious exception; in a polarization where $\cos\gamma = 0$ only symmetrical profiles are reproducible.

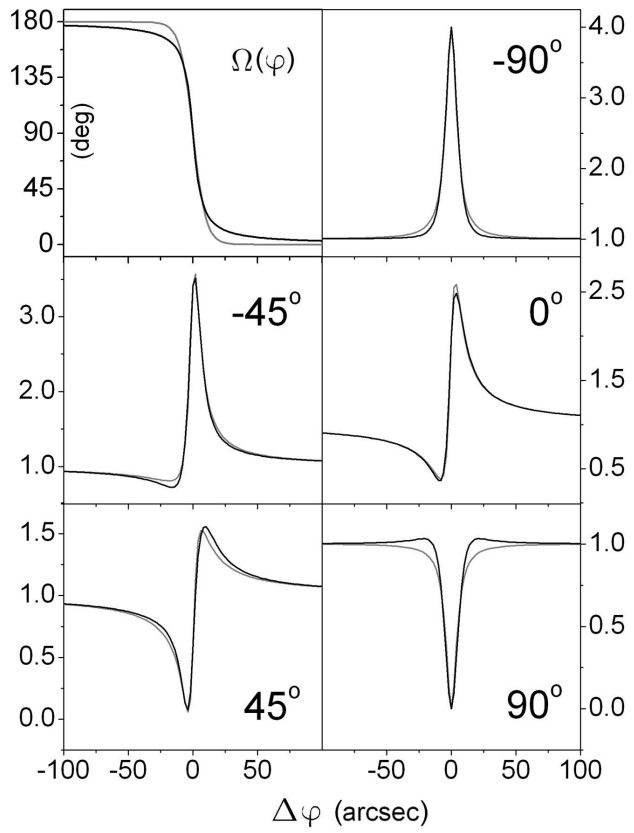

Figure 2
Behavior of possible functions for describing the dynamical phase shift, $\Omega(\varphi)$, and their effects on some interference profiles. Top-left plot: $\Omega(\varphi)$ function, 'out $\rightarrow$ in' sense, from equation (8) (dark line) and $\Omega(\varphi) = \pi/2\{1 - \tanh[(\varphi - \varphi_0)/w]\}$ from Shen *et al.* (2000) (gray line). Other plots: interference profiles simulated with the phase shift functions, dark and gray lines, respectively, for $\delta_T = -90, -45, 0, 45$, and 90° (given at the right-hand side of each plot). The profiles were generated by equation (5) with $w = 10''$, $R = 1$, $b = 0$ and $v_P = v_D = 1$. Horizontal coordinate is $\Delta\varphi = \varphi - \varphi_0$. A further comparison can also be done with the dynamical phase shift and interference profiles given in Figs. 5 and 6 of Weckert & Hümmer (1997).

Restricted to primary reflections in Bragg diffraction geometry, which avoid effects due to *Pendellösung* (Thorkildsen *et al.*, 2001), and except for interference fringes in the profiles of crystals with finite thickness, equation (5) is capable of fitting any profile whether it has an *Umweg* (peak-like) or an *Aufhellung* (dip-like) character; some examples were given in the paper by Morelhão & Kycia (2002). The real problem is that very different values of triplet phases can be assigned to the same profile. This means that a given profile does not correspond to a single point in the six-dimensional space of parameter vectors $\mathbf{p} = [\varphi_0, w, R, \xi, b, \delta_T]$. Note that, even restricted to *Umweg* cases ($b = 0$), the detector reading of the detoured beam, $P_D(\varphi)$, in (3) is an unknown quantity represented by the parameter R in (5). It must also be determined, together with ξ and δ_T, by fitting experimental profiles. This is a task that cannot be unequivocally accomplished. Just as numerical examples, the parameter vectors $\mathbf{p}_1 = [\varphi_0, w, R = 1, \xi = 0.4, b = 0, \delta_T]$ and $\mathbf{p}_2 = [\varphi_0, w, R, \xi = 1, b = 0, \delta_T]$ can be replaced in (5) to see that they do generate the same $P(\varphi)$ profiles, but each value of δ_T in $\mathbf{p}_1$, $[\delta_T]_1$, corresponds to a different pair of R and δ_T values in $\mathbf{p}_2$, $[R, \delta_T]_2$. For instance, with $v_P = v_D = 1$, $\varphi_0 = 0$, $w = 10''$ and the 'out–in' line profile function: $[-90^\circ]_1 \leftrightarrow [0.67, -90^\circ]_2$, $[-45^\circ]_1 \leftrightarrow [0.64, -64^\circ]_2$, $[0^\circ]_1 \leftrightarrow [0.54, -40^\circ]_2$, $[45^\circ]_1 \leftrightarrow [0.32, -30^\circ]_2$ and $[90^\circ]_1 \leftrightarrow [0.095, -90^\circ]_2$ – this last example resembles the profile reversal effect due to crystal imperfections ($\xi < 1$) pointed out by Larsen & Thorkildsen (1998). The above examples illustrate the systematic errors that can be obtained in δ_T when assuming $\xi = 1$ in (5). Therefore, although (5) can reproduce almost any interference profile and also take into account effects of crystalline imperfections, it is useless to extract the phase from a single 3-BD profile.

6. A three-beam diffraction phasing procedure with synchrotron radiation

Synchrotron facilities today are available to almost any researcher, even in developing countries. So, proposing experiments that must be carried out exclusively with synchrotron radiation is not a problem. The natural linear polarization of synchrotron radiation can tune the polarization coefficients of (5) in order to break the degeneracy of its parameters. It allows the asymmetric/symmetric decomposition of $P(\varphi)$ specified by (6) and then elimination of systematic errors in measuring δ_T due to symmetric distortions of the profiles. Relevant features of (5) to be outlined are:

(i) when $v_P \simeq 0$, the maximum of $P(\varphi)$ is very much determined by the value of R;

(ii) *Aufhellung* distortions, *i.e.* the value of b, are significant when $v_P \simeq 1$ and/or $v_D \simeq 0$;

(iii) polarization directions in which $v_P \simeq R v_D$ and $|\cos\gamma| \simeq 1$ are the most sensitive ones to the values of ξ and δ_T;

(iv) as a function of polarization, the contributions to $P(\varphi)$ from the interference term and from $P_\wedge(\varphi)$ are different since their weights vary with $v_P v_D \cos\gamma$ and with v_P^2 and v_D^2, respectively;

(v) The φ range of $P_{\sim}(\varphi)$ is wider than $P_{\wedge}(\varphi)$ since $|f(\varphi_0 + \Delta\varphi)| > |f(\varphi_0 + \Delta\varphi)|^2$. It increases the sensitivity to the asymmetric component of $P(\varphi)$.

These features suggest the possibility of developing a phasing procedure where the triplet phases are, in principle, measured by using (5) to fit sets of φ scans taken at different polarization, for instance, with v_P varying from 0 to 1 and passing through the condition specified in (iii).

Conflicts between diffraction theories arrive at this point and can lead to equivocal implementation of the above-mentioned procedure, and consequently to loss of accuracy in determining δ_T. According to the deduction of (5), which only considers A and $B + C$ as *Umweg* channels, the R and ξ parameters should have constant values as a function of v_P and v_D, and then all φ scans of a given data set have to be fitted with the same values of R and ξ. The b parameter could also be constant in the data set by considering only B and $A + \bar{C}$ as *Aufhellung* channels and taking the polarization coefficients of these channels into account, as shown in the Appendix of Morelhão (2003). These two pairs of channels provide the second- and third-order approximations to the 3-BD phenomenon. Even then, the R, ξ and b parameters can present smooth variations as a function of the polarization owing to diffraction of higher-order channels. Instrumental effects can also contribute to the variations of some of these parameters. Therefore, as a general rule, none of these parameters are global variables in the sets of φ scans – this is a revision of suggestions in earlier papers (Morelhão & Kycia, 2002; Morelhão, 2003). Although, eventually, an accurate value of the triplet phase can be obtained by assuming that some of them are constants. The only true global variable is the triplet phase itself.

Well elaborated computer algorithms capable of extracting the value of δ_T from a polarization-dependent set of φ scans have not yet been developed. Based on the arguments outlined above, the algorithm has to find the parameter vector, $\mathbf{p} = [\varphi_0, w, R, \xi, b, \delta_T]$, of each φ scan that provides the best possible fitting for a given value of δ_T. Since δ_T is common to all φ scans, the algorithm also has to search for the value of δ_T that allows the whole data set to be fitted. No constraints should be set to φ_0, w, R, ξ and b in any fitting, but some limited range of variation can be imposed, as for the value of R, which should be kept close to the value obtained by condition (i) mentioned above. An extra parameter due to instrumental broadening can also be included in $\mathbf{p}$ and, as far as it represents a symmetrical function of φ, no systematic errors will be generated in δ_T. The task suggested here for such an algorithm is impossible to accomplish by manual fitting of the φ scans. Even to a computer, it is an enormous task. To give an idea, if the data set is composed of six φ scans, there will be 37 parameters ($6 \times 6 + 1$: 6 scans, 6 parameters to each scan, and δ_T to whole data set) to be adjusted by the algorithm. Developing an algorithm to accomplish such a task is an open opportunity in this field of research.

To provide some theoretical evidence that it is worth investing effort in developing a phasing algorithm based on (5), the proposed procedure will be applied to a few sets of simulated φ scans, for perfect and non-perfect crystals. The latter is obtained by artificially adding symmetric positive curves to those from a perfect crystal. Note that for such a demonstration of phasing equation (5) itself could generate the simulated φ scans to be used as the input data. Instead, the dynamical theory of n-beam diffraction is used. There are some reasons for this choice, besides giving more credibility to the procedure. *Reason 1*: figure out if the parameter ξ is also required for fitting the profiles of a perfect crystal or if it can be assumed as zero *a priori*; *Reason 2*: when thickness fringes are present in the profiles, verify if after convolution with an instrumental broadening function the asymmetry of the final profile still preserves the phase information; and *Reason 3*: checking if the b parameter can properly take *Aufhellung* into account.

7. Theoretical results

7.1. Dynamical simulation of three-beam diffraction

The n-beam diffraction of X-rays in crystals, when treated by the plane-wave dynamical theory of diffraction, is basically a problem of solving the eigenvalues and eigenvectors of a $2n \times 2n$ square matrix, the so-called fundamental equations of the dynamical theory. They are derived from Maxwell's equations in a medium where the complex dielectric susceptibility is periodic. The eigenvalues are the changes in the wavevector components, along the crystal surface-normal direction, of the allowed propagation modes for X-ray waves; and the eigenvectors are the σ and π components of the wavefields assigned to each propagation mode. Here, for a given crystal orientation, the eigenvalues and eigenvectors are calculated according to Colella's formalism (Colella, 1974). The intensities, I_n ($n = 0, A, B$), of the diffracted beams from a

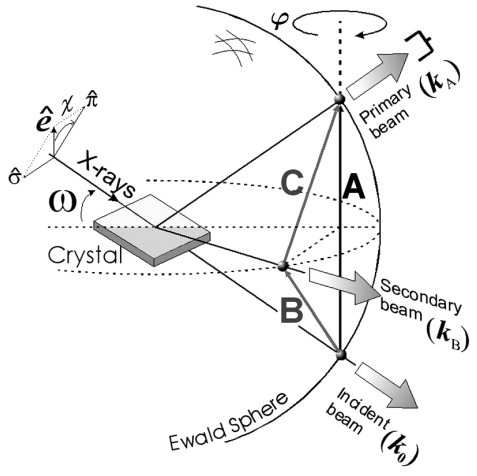

Figure 3
Reciprocal-space Ewald construction of the three-beam diffraction used here for demonstrative phasing purposes. **A**, **B** and **C** correspond to the diffraction vectors of the $\bar{2}26$ (primary), $\bar{3}\bar{1}3$ (secondary) and 133 (coupling) reflections of a cubic lattice. $\mathbf{k}_A$ and $\mathbf{k}_B$ are Bragg-reflected beams since the outward surface normal is 001. The φ axis is along the diffraction vector **A** and $\hat{e} = \sin\chi\hat{\sigma} - \cos\chi\hat{\pi}$ is the polarization direction of the incident beam where $\hat{\sigma} = \hat{k}_0 \times \hat{k}_A / \sin 2\theta_A$ and $\hat{\pi} = \hat{\sigma} \times \hat{k}_0$.

crystal plate are obtained by matching the total σ and π components of the propagation modes with the σ and π components of the incident and diffracted beams at both crystal surfaces (top/bottom), as described by Chang (1984). It is equivalent, in practice, to applying the boundary conditions of the electromagnetic fields at both surfaces, as used by Weckert & Hümmer (1997). Experimental parameters like divergence, spectral bandwidth and mosaicity are usually taken into account by convoluting the plane-wave dynamical profiles with a broadening function. This procedure is also adopted here. The intensity profiles of the primary beam ($n = A$) as a function of the crystal φ rotation is obtained after convolution with a Gaussian (FWHM = 11″), *i.e.*

$$P_{\rm Dyn}(\varphi) = \int_{-\infty}^{+\infty} I_A(\varphi - u)G(u)\,{\rm d}u. \qquad (9)$$

In Bragg diffraction geometry for a thin crystal, it is not necessary to integrate over the rocking-curve angle of the primary reflection to observe the interference effect in the φ scans. The effect is present at the maximum of the rocking curve, as pointed out by Weckert & Hümmer (1997).

The diffraction geometry of the particular 3-BD chosen for general comparison purposes is depicted in Fig. 3. It consists of two Bragg-reflected beams in a 2 µm thick plate of a cubic crystal where $\lambda/a = 0.2132$ (wavelength/lattice parameter). The primary (A), secondary (B) and coupling (C) reflections are $\bar{2}26$, $\bar{3}\bar{1}3$ and 133, respectively, and the outward surface normal is 001. The modulus and phase of the structure factors assigned to these reflections are $|F_A| = 44$, $|F_B| = |F_C| = 152$, $F_{000} = 328$, $\delta_A = 0$ and $\delta_B = \delta_C = 20°$. Then, the triplet phase value is $\delta_T = 40°$. The polarization angle, χ, specifies the polarization direction of the incident beam according to the definition given in Fig. 3. Fig. 4(*a*) shows the φ scans as a function of χ for the 'out–in' rotation sense, equation (8). Another set of dynamical φ scans, calculated for $|F_A| = 88$ – the only difference with those in Fig. 4(*a*) – is shown in Fig. 4(*b*). For the sake of simplicity, let us call $P_{\rm Dyn4}(\varphi)$ and $P_{\rm Dyn8}(\varphi)$ the dynamical profiles (φ scans) simulated with $|F_A| = 44$ and $|F_A| = 88$, respectively, while $P_{\rm Dyn}(\varphi)$ will refer to both.

7.2. Fitting dynamical profiles with the general parametric equation

Fitting procedures always request an error function to guide their improvement. The profiles $P(\varphi)$ generated by (5) have been compared to the dynamical φ scans, $P_{\rm Dyn}(\varphi)$ in Fig. 4, by means of the error function

$$E_\chi(\mathbf{p}) = (N-1)^{-1} \sum_{n=1}^{N} |P(\varphi_n, \mathbf{p}) - P_{\rm Dyn}(\varphi_n)|, \qquad (10)$$

where $\mathbf{p} = [\Delta\varphi_0, w, R, \xi, b, \delta_T]$ is the vector of adjustable parameters for a given polarization angle χ and N is the total number of data points in the scan. $\Delta\varphi_0$ is a correction in the theoretical center of the curves, $\varphi_{0,B}$, when calculated by Bragg's law (Cole *et al.*, 1962), so that $\varphi_0 = \varphi_{0,B} + \Delta\varphi_0$ in (8).

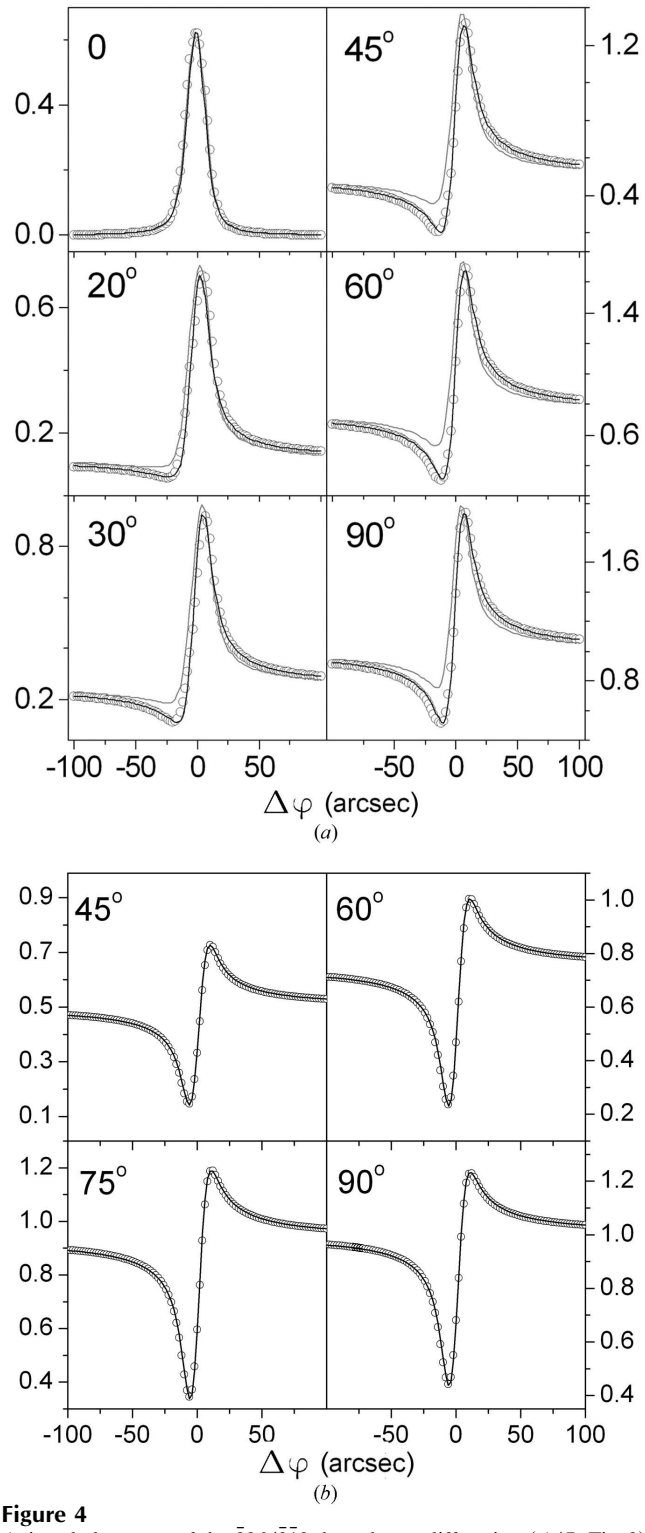

Figure 4
Azimuthal φ scans of the $\bar{2}26/\bar{3}\bar{1}3$ three-beam diffraction (A/B, Fig. 3) as a function of the polarization angle χ, whose values are shown at the left-hand side of each curve. Open circles: simulated data by the n-beam dynamical theory, equation (9). (*a*) $P_{\rm Dyn4}(\varphi)$ ($|F_A| = 44$) and (*b*) $P_{\rm Dyn8}(\varphi)$ ($|F_A| = 88$), see §7.1 for more details. Dark lines: best-fitting $P(\varphi)$ curves generated by equation (5) with the parameter vectors given in Table 1. Gray lines: $P_{\rm nPC}(\varphi)$ standing for the profiles of a non-perfect crystal artificially generated by adding an extra $\frac{1}{2}P(\varphi, \xi = 0, b = 0)$ symmetrical contribution to $P_{\rm Dyn4}(\varphi)$. All sets of profiles have been normalized by the respective maximum of the primary intensity obtained when $\chi = 90°$. $\Delta\varphi = \varphi - \varphi_0$.

Table 1
Parameter vectors $\mathbf{p} = [\Delta\varphi_0, w, R, \xi, b, \delta_T]$ of $P(\varphi)$, equation (5), used to reproduce $P_{\rm Dyn4}(\varphi)$, $P_{\rm nPC}(\varphi)$ and $P_{\rm Dyn8}(\varphi)$ at different polarization angles, χ, and for a common value of the triplet phase, $\delta_T = 40^\circ$.

The sets of dynamical profiles $P_{\rm Dyn4}(\varphi)$ and $P_{\rm Dyn8}(\varphi)$ were calculated for $|F_A| = 44$ and $|F_A| = 88$, respectively. $\Delta\varphi_0$ and w are in arcseconds. $1 - \xi^2$ and b stand for the quantities of positive and negative symmetrical components of the profiles, as defined in $P_\wedge(\varphi)$, equation (6*b*). R_0 is a reference value defined in §7.2.

	$P_{\rm Dyn4}(\varphi)$				$P_{\rm nPC}(\varphi)$		$P_{\rm Dyn8}(\varphi)$			
χ (°)	$\Delta\varphi_0$	w	R/R_0	$1-\xi^2$	R/R_0	$1-\xi^2$	$\Delta\varphi_0$	w	R/R_0	b
0	−1.2	9.7	1.23	–	1.23	–	−1.2	9.7	1.23	–
20	−0.7	10.4	1.12	0.29	1.11	0.67	–	–	–	–
30	0.3	9.7	1.16	0.26	1.14	0.66	–	–	–	–
45	1.2	9.4	1.18	0.24	1.18	0.62	1.4	6.5	1.29	0.42
60	1.2	8.6	1.22	0.19	1.22	0.59	−1.4	6.5	1.27	0.45
75	0.9	8.3	1.24	0.17	1.24	0.58	−1.4	6.5	1.25	0.46
90	0.6	7.9	1.27	0.14	1.27	0.57	−1.4	6.5	1.23	0.41
	$b = 0$, $R_0 = 1.6864$						$\xi = 1$, $R_0 = 0.9434$			

Before calculating $E_\chi(\mathbf{p})$, $P(\varphi)$ is also convoluted with the instrumental Gaussian (FWHM = 11″) as in (9).

Since the Bragg angle of the primary reflection has been set to 45°, the ξ, b and δ_T parameters do not affect the profile of the simulated φ scan at $\chi = 0$. Then, the R/R_0 ratio can be unequivocally determined from peak fitting. R_0 is a reference value obtained from the maximum of the peak as $[P_{\rm Dyn}(\varphi_0)]^{1/2}/v_D$. For the $P_{\rm Dyn}(\varphi)$ sets in Fig. 4, $R_0 = 1.6864$ ($|F_A| = 44$) or $R_0 = 0.9434$ ($|F_A| = 88$). Note that in the absence of dynamical diffraction effects (primary extinction) $R/R_0 = 1$ regardless of the state of linear polarization.

The versatility of (5) in fitting profiles taken at different polarization ($\chi \neq 0$) allows all dynamical φ scans in Fig. 4, $P_{\rm Dyn}(\varphi)$ (open circles), to be fitted with the same δ_T value, which is known in this case. Then, with $\delta_T = 40^\circ$, the other parameters of p are adjusted to minimize the error function. The $P_{\rm Dyn4}(\varphi)$ profiles (Fig. 4*a*) are reproduced with $b = 0$, and it makes the adjustment quite a simple procedure because R and ξ do affect, in the first order, the maximum and the minimum of the interference curves, respectively. On the other hand, the four $P_{\rm Dyn8}(\varphi)$ profiles (Fig. 4*b*) could not be reproduced with $b = 0$. Instead, they were reproduced by keeping $\xi = 1$ and adjusting R and b. The values of $\Delta\varphi_0$, w, R/R_0, $1 - \xi^2$ and b thus obtained are given in Table 1, and the respective best fitting $P(\varphi)$ curves (dark lines) are those compared to $P_{\rm Dyn}(\varphi)$ in Fig. 4.

To artificially simulate the effects of crystalline defects in 3-BD experiments, *i.e.* to simulate interference profiles of non-perfect crystals, $P_{\rm nPC}(\varphi)$, a symmetrical contribution of 50% (just a percentage between 0 and 100%) has been added to $P_{\rm Dyn4}(\varphi)$. In other words, $P_{\rm nPC}(\varphi) = P_{\rm Dyn4}(\varphi) + 0.5P(\varphi, \mathbf{p})$, where $\mathbf{p}$ is given in Table 1 but with $\xi = 0$. Both sets of profiles, $P_{\rm Dyn4}(\varphi)$ (open circles) and $P_{\rm nPC}(\varphi)$ (gray lines), are seen in Fig. 4(*a*). The intensities of their base lines correspond to the value of v_P^2 since they were normalized by the respective primary intensity obtained when $\chi = 90^\circ$ ($v_P \simeq 1$). Note that, after normalization, the addition of 50% actually represents 33% of symmetrical contribution. The fitting procedure of adjusting $\Delta\varphi_0$, w, R/R_0 and $1 - \xi^2$, while $\delta_T = 40^\circ$ and $b = 0$ was also applied to $P_{\rm nPC}(\varphi)$; the results are shown in Table 1 (columns 6 and 7). The respective values of $\Delta\varphi_0$ and w are not shown because they are the same as those in columns 2 and 3. Although the best-fitting curves for $P_{\rm nPC}(\varphi)$ are not shown in Fig. 4(*a*), the agreements are of the same quality as those obtained between $P(\varphi)$ and $P_{\rm Dyn4}(\varphi)$.

7.3. Examples of phasing procedures

Demonstrative phasing procedures are applied to the profiles in Fig. 4. They explore the fact that δ_T must have a common value for all φ scans, but it is assumed to be unknown. In the absence of efficient fitting and phasing algorithms, the procedures adopted here make use of predetermined values of $\Delta\varphi_0$ and w. Then, for a given δ_T, the error function, $E_\chi(\mathbf{p})$, of each φ scan is minimized by adjusting R and ξ ($b = 0$) or R and b ($\xi = 1$), and then added up to the collective error function

$$S(\delta_T) = \sum_{\chi \neq 0} E_\chi(\mathbf{p}). \qquad (11)$$

In fact, for the R and ξ parameters, the values of R/R_0 and $1 - \xi^2$ have been adjusted instead of R and ξ themselves. The adjustment consists of simple time-consuming double-loop computer routines that perform mesh scans with resolution of 0.01 in R/R_0 and $1 - \xi^2$ or in R/R_0 and b. The φ scan at $\chi = 0$ provides the value of R_0 but $E_0(\mathbf{p})$ is not considered in the sum of (11) because it is phase insensitive ($v_P \simeq 0$). Fig. 5 shows the minimization curves of $S(\delta_T)$ as a function of δ_T for all sets of profiles in Fig. 4, *i.e.* for $P_{\rm Dyn4}(\varphi)$ and $P_{\rm nPC}(\varphi)$, for their respective best-fitting $P(\varphi)$ profiles, and also for $P_{\rm Dyn8}(\varphi)$.

8. Discussion

Some features in the dynamical simulation of the chosen 3-BD case (Fig. 3) deserve a few comments: (i) A relatively weak primary reflection was necessary to reduce *Aufhellung* in the sets of $P_{\rm Dyn4}(\varphi)$ and $P_{\rm nPC}(\varphi)$ profiles. It allows both sets to be fitted with $b = 0$, which was helpful in demonstrating that the ξ parameter can properly take into account a symmetric positive distortion of the profiles; for example, the comparison of columns 5 and 7 of Table 1. When the strength of the primary reflection is increased, from $|F_A| = 44$ to $|F_A| = 88$, *Aufhellung* becomes more significant, so that the $P_{\rm Dyn8}(\varphi)$ profiles cannot be reproduced with $b = 0$. (ii) The triplet phase value of 40°

has been chosen mostly to enhance the visual effects of the asymmetries in the $P_{\rm Dyn4}(\varphi)$ and $P_{\rm nPC}(\varphi)$ profiles. Since the primary reflection is weak and the crystal very thin, a triplet phase value of, for instance, -60° would produce nearly symmetric positive profiles even at σ polarization ($\chi = 90^\circ$). It does not make any difference to the phasing procedures, but all profiles in Fig. 4(*a*) would be very like the one at $\chi = 0$. (iii) The primary reflection axis, $[\bar{1}13]$, tilted from the surface-normal direction, [001], avoids the Bragg-surface diffraction geometry. This particular geometry makes the simulation of the profiles by the *n*-beam dynamical theory significantly more complicated (Avanci & Morelhão, 2000). (iv) The numerical precision required for solving the equations of the *n*-beam dynamical theory have also limited the crystal thickness. (v) The Gaussian width (FWHM) of $11''$ was the minimum value necessary to average out the thickness fringes of the dynamical profiles. The total integration range in (9) is 3 FWHM.

8.1. Symmetric/asymmetric decomposition of the interference profiles

The $1 - \xi^2$ quantities of the symmetrical component found in $P_{\rm Dyn4}(\varphi)$, column 5 of Table 1, are intrinsic of the dynamical diffraction simulation specified in §7.1. Any change in thickness, phase, scattering geometry, experimental parameters (Gaussian width), ... can change the values of these intrinsic quantities. For phasing procedures based on equation (5), the fact of finding $\xi < 1$, even in perfect crystals, is not a problem, as far as this parameter is not assumed equal to 1 *a priori*. The important fact is that, when arbitrary quantities of symmetric positive components are added to the profiles, the ξ parameter does account for these extra quantities as shown by the values in column 7 (Table 1). It demonstrates the potential of the approach in decomposing the profiles into their symmetric and asymmetric components, as given in equation (6), without affecting the triplet phase values. This is the fundamental fact that certifies this proposal of phasing procedures for non-perfect crystals.

The majority of the parameter values listed in Table 1 vary as a function of the polarization angle. Since in the fittings, for $\chi \neq 0$, ξ and b parameters were not simultaneously adjusted, the exact interpretation of the observed variations are very difficult. There is a correlation between them, in the sense that the total amount of symmetrical distortion, $P_\wedge(\varphi)$ [equation (6*b*)], is the result of the sum of positive and negative components, respectively determined by $1 - \xi^2$ and b. It is important to note that these components have different dependencies with the polarization angle, as already pointed out [see (iv) in §6]. The product ξR in $P_\sim(\varphi)$ [equation (6*a*)] establishes the correlation between ξ and R. Then, as one parameter is kept constant, variations as a function of polarization are observed in the other parameters. Besides, third-order *Umweg* channels (those given in §2 with three bounces) do involve the reflection A, whose polarization coefficient, v_P, varies significantly with χ. It is an expected source of variation to R. One last fact to consider is the effect of the Gaussian convolution with the thickness fringes, whose amplitude patterns also change with polarization. This effect is probably related to the observed variations in $\Delta\varphi_0$ and w, as well as to the intrinsic $1 - \xi^2$ quantities of the symmetrical component found in the dynamical profiles.

Although a detailed understanding of the reasons behind the variations of $\Delta\varphi_0$, w, R, ξ and b can be quite interesting, it is not of practical relevance. Each 3-BD case, when investigated theoretically or experimentally by equation (5), can present completely different sets of parameter vectors. The real challenge is how to determine the triplet phases by systematic procedures, starting with no clue on the values of the parameters or even on their range of variation. Any attempt to apply (5) for phasing purposes, whether for experimental or simulated data sets, brings more information to the knowledge of how to develop the procedures. That is the objective of the phasing attempts described in §7.3, as discussed below.

8.2. Accuracy of the phasing procedures

For a given set of polarization-dependent φ scans, as soon as the direction of the beams ($\mathbf{k}_0$, $\mathbf{k}_A$ and $\mathbf{k}_B$; Fig. 3) and the rotation sense of the crystal are known, the triplet phase can be found in one of two intervals, M_1: $-90 < \delta_T < 90^\circ$ or M_2: $90 < \delta_{\rm T} < 270^\circ$. The criteria, deducible from the profiles in Fig. 2, are the following:

(i) $\{P(\varphi_0 - \Delta\varphi) < P(\varphi_0 + \Delta\varphi)$ and 'out $\rightarrow$ in'$\}$ or $\{P(\varphi_0 - \Delta\varphi) > P(\varphi_0 + \Delta\varphi)$ and 'in $\rightarrow$ out'$\} \Rightarrow M_1$;

(ii) $\{P(\varphi_0 - \Delta\varphi) > P(\varphi_0 + \Delta\varphi)$ and 'out $\rightarrow$ in'$\}$ or $\{P(\varphi_0 - \Delta\varphi) < P(\varphi_0 + \Delta\varphi)$ and 'in $\rightarrow$ out'$\} \Rightarrow M_2$;

where $\Delta\varphi > 0$, and the expressions 'out $\rightarrow$ in' and 'in $\rightarrow$ out' are defined in equation (8). Note that this criterion is for $\cos\gamma > 0$ in equation (5), otherwise the above relationships are reversed, (i) $\Rightarrow M_2$ and (ii) $\Rightarrow M_1$ for $\cos\gamma < 0$.

A second step in the procedure is to determine R_0. In the $\pi/2$ scattering geometry ($\mathbf{k}_0 \cdot \mathbf{k}_A = 0$), R_0 is measured from the φ scan with π polarization ($\chi = 0$). Knowledge of the R_0 value allows the adjustment of R/R_0 to be restricted to values close to 1. The minimizations of the collective error functions in Fig. 5 were carried out with $1 \leq R/R_0 \leq 1.4$.

Establishing constraints to the variation to R/R_0 is one of the most important points in the procedure to avoid systematic errors. In the numerical examples given at the end of §5, the profiles generated with the parameter vector $\mathbf{p}_1$ could be reproduced with $\mathbf{p}_2$ just because the values of R were freely adjusted. Once R/R_0 is properly constrained, systematic errors are eliminated and the final accuracy in δ_T depends on particularities of each 3-BD case such as the quantities of symmetric positive components (crystal imperfections) and the relative strengths of the primary and detour waves, *i.e.* the value of R_0 itself. The values assigned to $\Delta\varphi_0$ and w of each φ scan also affect the final accuracy.

Minimization of $S(\delta_T)$ for $P(\varphi)$ profiles (as input data) provides a sense of the maximum accuracy that can be achieved in triplet phase determination. Such minimization curves show the inherent phase sensitiveness of a given 3-BD case. It is because there will be a set of parameter vectors that

exactly reproduce the profiles ($S = 0$). For the case exploited here, these $S(\delta_T)$ curves (gray symbols in Figs. 5*a* and 5*b*) were calculated for the best-fitting $P(\varphi)$ profiles of $P_{\rm Dyn4}(\varphi)$ and $P_{\rm nPC}(\varphi)$. The relevant point to stress is that, although the minima occur at 40°, they are not well pronounced. The minima are flats and their widths establish the maximum possible accuracy, or the inherent accuracy, for each set of profiles, which are ±5 and ±15° for the $P_{\rm Dyn4}(\varphi)$ and $P_{\rm nPC}(\varphi)$ sets, respectively.

The dynamical $P_{\rm Dyn4}(\varphi)$ profiles, Fig. 4(*a*), present different values of $\Delta\varphi_0$ and w when analyzed by equation (5). It is helpful to demonstrate how estimating the values of these two parameters can compromise accuracy. When their values are mistaken, there is a loss in accuracy that can be seen by comparing the two minimization curves in Fig. 5(*a*). With $\Delta\varphi_0 = -1.2''$ and $w = 9.7''$ assigned to all φ scans, the accuracy is about ±10° against the inherent one of ±5°. In Fig. 5(*b*), both curves (open and gray squares) provided the same accuracy, since the predetermined values of $\Delta\varphi_0$ and w (columns 2 and 3 of Table 1) were used to minimize $S(\delta_T)$ for the $P_{\rm nPC}(\varphi)$ profiles.

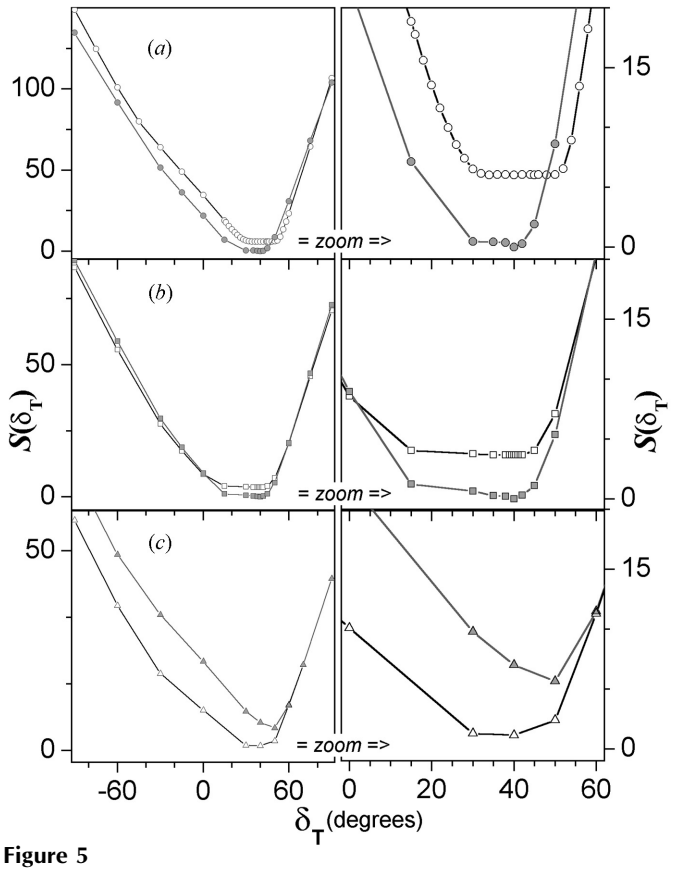

Figure 5
Minimization of the collective error function, $S(\delta_T)$ [equation (11)], for the polarization-dependent sets of φ scans in Fig. 4: (*a*) $P_{\rm Dyn4}(\varphi)$; (*b*) $P_{\rm nPC}(\varphi)$; (*c*) $P_{\rm Dyn8}(\varphi)$. In (*a*) and (*b*), R/R_0 and $1 - \xi^2$ of each φ scan is adjusted with $b = 0$, and the sum in $S(\delta_T)$ goes over $\chi = 20, 30, 45, 60, 75$ (not shown in Fig. 4*a*) and 90°. Curves with open symbols (circles and squares only) stand for fittings where: (*a*) $\Delta\varphi_0 = -1.2''$ and $w = 9.7''$ for all φ scans (first row of Table 1, $\chi = 0°$); and (*b*) $\Delta\varphi_0$ and w values are those predetermined in columns 2 and 3 of Table 1. On the other hand, curves with gray symbols (circles and squares only) are the minimization of $S(\delta_T)$ for the respective best-fitting $P(\varphi)$ profiles (Table 1). The gray curves in (*a*) and (*b*) represent the maximum possible accuracy on which δ_T can be determined for this 3-BD case, whose triplet phase value is 40°. In (*c*), the sum goes over $\chi = 45$, 60, 75, and 90° (Fig. 4*b*), and R/R_0 and $1 - \xi^2$ ($b = 0$) are adjusted only for the curve with gray triangles, while R/R_0 and b ($\xi = 1$) are the adjustable parameters for the $S(\delta_T)$ curve with open triangles. $\Delta\varphi_0$ and w values are those predetermined in columns 8 and 9 of Table 1.

It follows directly from equation (5) that a small value of ξ reduces the contribution of the interference term into $P(\varphi)$ and then the sensitivity to determine δ_T. The profiles of a non-perfect crystal, $P_{\rm nPC}(\varphi)$ in Fig. 4(*b*), have 33% of symmetrical contribution. It provides a reduction of about 30% in the values of ξ, calculated from columns 5 and 7 of Table 1. Consequently, there is a loss of accuracy that can be noted by comparing the inherent accuracy of the $P_{\rm Dyn4}(\varphi)$ and $P_{\rm nPC}(\varphi)$ sets of profiles, ±5 and ±15°, respectively. The $S(\delta_T)$ curve in Fig. 5(*b*), for $P_{\rm nPC}(\varphi)$, is minimized around the expected triplet phase value of 40°. Therefore, it demonstrates that the flexibility of equation (5), owing to the ξ parameter, eliminates systematic errors due to crystalline imperfections; errors such as those observed in the numerical examples at the end of §5. However, the phase sensitiveness is reduced as the quantity of symmetrical distortion increases.

Indirectly, the value of R_0 also affects the phase sensitiveness. If $R_0 > 1/v_D$, the condition specified in (iii) of §6 cannot be fulfilled. Although *Aufhellung* is significant in the $P_{\rm Dyn8}(\varphi)$ profiles (Fig. 4*b*), the best accuracy in δ_T is observed for this set of profiles as seen by the $S(\delta_T)$ curve (open triangles) in Fig. 5(*c*). The reason may just be the value of $R_0 = 0.943$, which is smaller than the value of 1.686 measured in the other sets of profiles.

The final example to consider is the situation where it is not obvious which of the ξ and b parameters can be fixed or if both need to be adjusted to fit the whole set of φ scans. This dilemma can be solved by carrying out two minimizations of $S(\delta_T)$, one where $b = 0$ and another where $\xi = 1$. Fig. 5(*c*) shows both $S(\delta_T)$ curves for the $P_{\rm Dyn8}(\varphi)$ profiles. With $b = 0$ (gray triangles), there is a minimum close to $\delta_T = 50°$ but the fits are of poor quality. On the other hand, with $\xi = 1$ (open triangles), the minimum is at the right δ_T value, and the very good fits shown in Fig. 4(*b*) are achieved. $P_{\rm Dyn8}(\varphi)$ profiles at polarization angles smaller than 45°, as $\chi = 20$ and 30°, could not be fitted in any of these two hypotheses ($b = 0$ or $\xi = 1$), and then they were not included in the sum of $S(\delta_T)$. To include them in the sum, it would necessarily be a minimization scheme where R/R_0, ξ and b are simultaneously adjusted

8.3. Final remarks

The phasing procedures demonstrated above can be applied, in principle, to crystals with completely unknown structures. However, 3-BD cases must be identified among other cases of n-BD ($n > 3$), and the direction of the secondary beam ($\mathbf{k}_B$, Fig. 3) determined. The procedures based on minimization of $S(\delta_T)$ implicitly assume that all asymmetries of the 3-BD profiles are due to interference of photons scattered by *Umweg* channels. Any extra feature that can induce

asymmetrical changes in the characteristic profiles must be carefully investigated. As reported in the literature (Thorkildsen *et al.*, 2001, and references therein), the 3-BD profiles of Laue cases (transmitted primary beam) are strongly influenced by the *Pendellösung* effects depending on the thickness of the crystal. Therefore, for these cases, the viability of the suggested phasing procedure depends on crystal thickness.

Applications of the phasing procedures in practice, *i.e.* in experimental sets of φ scans, add in a few minor instrumental difficulties that have to be overcome. Tiny misalignments of the experimental set-up, in general, do produce small shifts in $\Delta\varphi_0$ as a function of χ. Any manual assignment of values to $\Delta\varphi_0$ (of each φ scan) does certainly compromise accuracy, as demonstrated in Fig. 5(*a*). In most synchrotron beamlines, the X-ray optics is different in horizontal and vertical scattering planes. It implies that the width of the instrumental broadening function, which convolutes with the intrinsic width w in equation (9), is different at each polarization. Statistical noise in radiation detection certainly raises the minimum values of the error functions, but it does not directly imply loss of accuracy. To properly consider such minor difficulties, the minimization schemes of $S(\delta_T)$ must also include $\Delta\varphi_0$, w and instrumental widths adjustable to each φ scan. It emphasizes how important the algorithm outlined in §6 is for practical applications of the phasing procedures suggested in this article. Only with such an algorithm in hand can the practical validity of the procedures be verified for a wide range of 3-BD cases and the relevance of secondary features, as statistic noise and background corrections will then be properly investigated.

9. Conclusions

In this article, a general parametric equation for fitting interference profiles of three-beam X-ray diffraction is proposed. The profiles are decomposed in asymmetric and symmetric components when analyzed by the equation. It allows relatively accurate triplet phase determination in perfect as well as in non-perfect crystals. The concept of non-perfect crystals is restricted to those where crystalline imperfections only provide extra amounts of the symmetrical component in the interference profiles. The symmetrical components cannot be unequivocally identified from a single φ scan. Therefore, a phasing procedure is also suggested. It consists in collecting a polarization-dependent set of φ scans and minimization of the collective error function. The great advantage of the procedure relies on its potential to be carried out completely automatically in crystals with unknown structures and to provide a sense of the accuracy of the measured triplet phases.

The author would like to thank S. Kycia for valuable discussions as well as Márcia Fantini for the very kind and valuable revisions of the manuscript. This work was supported by the Brazilian founding agencies FAPESP (Grant no. 02/10387-5) and CNPq (Proc. no. 301617/95-3).

References

Authier, A. (1986). *Acta Cryst.* A**42**, 414–426.
Avanci, L. H. & Morelhão, S. L. (2000). *Acta Cryst.* A**56**, 507–508.
Chang, S. L. (1982). *Phys. Rev. Lett.* **48**, 163–166.
Chang, S. L. (1984). *Multiple Diffraction of X-rays in Crystals.* Heidelberg: Springer-Verlag.
Chang, S. L. & Tang, M. T. (1988). *Acta Cryst.* A**44**, 1065–1072.
Cole, H., Chambers, F. W. & Dunn, H. M. (1962). *Acta Cryst.* **15**, 138–144.
Colella, R. (1974). *Acta Cryst.* A**30**, 413–423.
Hart, M. & Lang, A. R. (1961). *Phys. Rev. Lett.* **7**, 120–121.
Høier, R. & Marthinsen, K. (1983). *Acta Cryst.* A**39**, 854–860.
Juretschke, W. J. (1986). *Acta Cryst.* A**42**, 449–456.
Larsen, H. B. & Thorkildsen, G. (1998). *Acta Cryst.* A**54**, 137–145.
Morelhão, S. L. (2003). *J. Synchrotron Rad.* **10**, 236–241.
Morelhão, S. L. & Avanci, L. H. (2001). *Acta Cryst.* A**57**, 192–196.
Morelhão, S. L., Härtwig, J. & Meier, D. L. (2000). *J. Cryst Growth*, **213**, 288–298.
Morelhão, S. L. & Kycia, S. (2002). *Phys. Rev. Lett.* **89**, 015501.
Okitsu, K. (2003). *Acta Cryst.* A**59**, 235–244.
Post, B. (1977). *Phys. Rev. Lett.* **39**, 760–763.
Renninger, M. (1937). *Z. Kristallogr.* **97**, 107–121.
Shen, Q. (1986). *Acta Cryst.* A**42**, 525–533.
Shen, Q. & Colella, R. (1987). *Nature (London)*, **329**, 232–233.
Shen, Q. & Colella, R. (1988). *Acta Cryst.* A**44**, 17–21.
Shen, Q., Kycia, S. & Dobrianov, I. (2000). *Acta Cryst.* A**56**, 268–279.
Stetsko, Yu. P., Juretschke, H. J., Huang, Y. S., Lee, Y. R., Lin, T. C. & Chang, S. L. (2001). *Acta Cryst.* A**57**, 359–367.
Thorkildsen, G., Larsen, H. B. & Weckert, E. (2001). *Acta Cryst.* A**57**, 389–394.
Tischler, J. Z. & Batterman, B. W. (1986). *Acta Cryst.* A**42**, 510–514.
Wagner, E. (1923). *Phys. Z.* **21**, 94–99.
Weckert, E. & Hümmer, K. (1997). *Acta Cryst.* A**53**, 108–143.